Energetic Constraints on the Position of the Intertropical Convergence Zone

TOBIAS BISCHOFF AND TAPIO SCHNEIDER

California Institute of Technology, Pasadena, California, and ETH Zurich, Zurich, Switzerland

(Manuscript received 22 October 2013, in final form 12 March 2014)

ABSTRACT

The intertropical convergence zone (ITCZ) can shift meridionally on seasonal and longer time scales. Previous studies have shown that the latitude of the ITCZ is negatively correlated with cross-equatorial atmospheric energy transport. For example, the ITCZ shifts southward as the Northern Hemisphere cools and the northward cross-equatorial energy transport strengthens in response. It has remained unclear what controls the sensitivity of the ITCZ position to cross-equatorial energy transport and what other factors may lead to shifts of the ITCZ position. Here it is shown that the sensitivity of the ITCZ position to cross-equatorial energy transport depends on the net energy input to the equatorial atmosphere: the net radiative energy input minus any energy uptake by the oceans. Changes in this energy input can also lead to ITCZ shifts. The cross-equatorial energy transport is related through a series of approximations to interhemispheric asymmetries in the near-surface temperature distribution. The resulting theory of the ITCZ position is tested in idealized general circulation model simulations with a slab ocean as lower boundary condition. In the simulations, cross-equatorial energy transport increases under global warming (primarily because extratropical latent energy fluxes strengthen), and this shifts the ITCZ poleward. The ITCZ shifts equatorward if primarily the tropics warm in response to an increased net energy input to the equatorial atmosphere. The results have implications for explaining the varied response of the ITCZ to global or primarily tropical changes in the atmospheric energy balance, such as those that occur under global warming or El Niño.

1. Introduction

The intertropical convergence zone (ITCZ) is a band of deep convective clouds in the tropics that marks the region of maximum precipitation on Earth. It is located around 6°N latitude in the annual and zonal mean but migrates seasonally between a more northern position in boreal summer and a more southern position in austral summer (Waliser and Gautier 1993; Adler et al. 2003; Berry and Reeder 2014). Additionally, the annual-mean position of the ITCZ has shifted on geological time scales (e.g., Haug et al. 2001; Arbuszewski et al. 2013), mimicking its seasonal migration insofar as it tends to shift toward a differentially warming and away from a differentially cooling hemisphere (e.g., Koutavas and Lynch-Stieglitz 2004; Chiang and Friedman 2012). Modeling studies with general circulation models (GCMs) have demonstrated that remote extratropical factors, such as the presence or absence of polar ice cover or high-latitude temperature variations caused by the Atlantic meridional overturning circulation, can lead to shifts of the ITCZ, generally away from a cooling and toward a warming hemisphere (e.g., Vellinga and Wood 2002; Chiang et al. 2003; Chiang and Bitz 2005; Broccoli et al. 2006; Yoshimori and Broccoli 2008).

Recent studies have focused on the role of the cross-equatorial energy transport and the atmospheric energy budget in controlling the ITCZ position. They have demonstrated that the ITCZ tends to shift southward as the northward atmospheric energy transport across the equator strengthens, for example, in response to a northern high-latitude cooling (e.g., Kang et al. 2008, 2009; Frierson and Hwang 2012; Donohoe et al. 2013, 2014). As the atmospheric energy transport generally strengthens in the direction of a cooling hemisphere, to partially compensate the cooling, the recent studies focusing on the atmospheric energy transport are broadly consistent with studies that emphasize surface temperature changes (e.g., Chiang et al. 2003; Chiang and Bitz 2005; Cvijanovic and Chiang 2013).

However, the ITCZ also shifts southward during El Niño (e.g., Dai and Wigley 2000; Berry and Reeder 2014),

Corresponding author address: Tobias Bischoff, Division of Geological and Planetary Sciences, 1200 E. California Blvd., Pasadena, CA 91125.
E-mail: tobias@caltech.edu

DOI: 10.1175/JCLI-D-13-00650.1

an observation not easily related to changes in cross-equatorial energy transport. A quantitative understanding of the factors controlling the ITCZ position, including the sensitivity of the ITCZ to changes in cross-equatorial energy transport, has remained elusive. That other factors than those hitherto considered must influence the ITCZ position is evident already for dimensional reasons: for example, it is empirically clear that the ITCZ position, which has units of length (e.g., displacement from the equator), is sensitive to the cross-equatorial atmospheric energy transport, which has units of power when integrated over latitude circles. To relate these two physical quantities, another quantity with units of power per unit length must enter any relation between ITCZ position and cross-equatorial energy transport.

Here we derive a quantitative relation between the cross-equatorial energy transport and the position of the ITCZ from the atmospheric energy balance. We show that the net energy input to the equatorial atmosphere is the natural quantity of units of power per unit of length to relate the ITCZ position to the cross-equatorial energy transport. We use an idealized GCM to demonstrate that the theoretically derived relation accurately captures the factors controlling the ITCZ position under both global and primarily tropical warming. The global and primarily tropical warming represent in an idealized manner aspects of what occurs under global warming associated with increased greenhouse gas concentrations and under more local tropical warming associated with changes in the tropical energy budget, such as occur during El Niño. We find that the ITCZ generally shifts away from the equator under global warming and toward the equator under primarily tropical warming.

However, other factors not taken into account in our simulations, such as differential changes in aerosol loading between the hemispheres (e.g., Rotstayn and Lohmann 2002; Hwang et al. 2013), likely would modulate the results we obtain in an idealized setting.

2. Theory

Atmospheric energy balance and energy transport

Neglecting the relatively small kinetic energy of atmospheric motions and energy storage in the atmosphere and on land surfaces, the zonal-mean energy balance integrated over atmospheric columns is (Neelin and Held 1987)

$$\mathcal{S} - \mathcal{L} - \mathcal{O} = \partial_y \langle \overline{vh} \rangle . \tag{1}$$

The left-hand side represents the net energy input to the atmosphere: the net incoming shortwave radiation $\mathcal{S}$ minus the outgoing longwave radiation $\mathcal{L}$ and any net energy uptake $\mathcal{O}$ by the oceans (or more generally the surface), associated with uptake/release of stored energy and/or ocean energy flux divergence. The right-hand side represents the divergence of the meridional flux (meridional velocity v) of moist static energy h in the atmosphere.[1] To simplify notation, we have adopted local Cartesian coordinates for small displacements $y = a\phi$ from the equator (Earth's radius a and latitude ϕ), suppressing $\cos(\phi)$ factors in the divergence; however, we perform all actual calculations in spherical coordinates. Angle brackets $\langle \cdot \rangle$ represent a mass-weighted integral over an atmospheric column, and overbars denote a time and zonal mean. Equation (1) states that any net energy input into the atmosphere must be balanced by a dynamic atmospheric energy transport from latitudes of net energy input (tropics) to latitudes of net energy deficit (extratropics).

At the ITCZ, low-level winds converge and upper-level winds diverge. To the extent that the latitude at which the mean meridional winds change sign does not vary strongly with altitude and that eddy fluxes across this latitude are negligible, the zonal-mean ITCZ is located close to the latitude δ at which the atmospheric energy flux $\langle \overline{vh} \rangle_\delta$ changes sign (e.g., Kang et al. 2008, 2009). The location of the zonal-mean precipitation maximum and the location where the atmospheric energy flux changes sign may not exactly coincide, and their separation may change with climate or seasons (Donohoe et al. 2013). We assume, however, that the responses in both quantities are correlated at least as long as the ITCZ remains close to the equator, and we focus on inferring the latitude where the atmospheric energy flux changes sign given the cross-equatorial energy transport and the net energy input to the tropical atmosphere. Expanding the atmospheric energy flux at a low-latitude δ around the cross-equatorial flux, we obtain, to first order in δ,

$$0 \approx \langle \overline{vh} \rangle_\delta = \langle \overline{vh} \rangle_0 + a\partial_y \langle \overline{vh} \rangle_0 \delta , \tag{2}$$

where the subscript 0 denotes quantities evaluated at the equator. Solving for δ and substituting for the atmospheric energy flux divergence [Eq. (1)] at the equator gives the ITCZ position

$$\delta \approx -\frac{1}{a} \frac{\langle \overline{vh} \rangle_0}{\mathcal{S}_0 - \mathcal{L}_0 - \mathcal{O}_0} . \tag{3}$$

[1] The moist static energy $h = s + l$ is defined as the sum of dry static energy $s = c_p T + gz$ and latent energy $l = L_v q$, where L_v is the latent heat of vaporization, q is the specific humidity, and other symbols have their usual meanings.

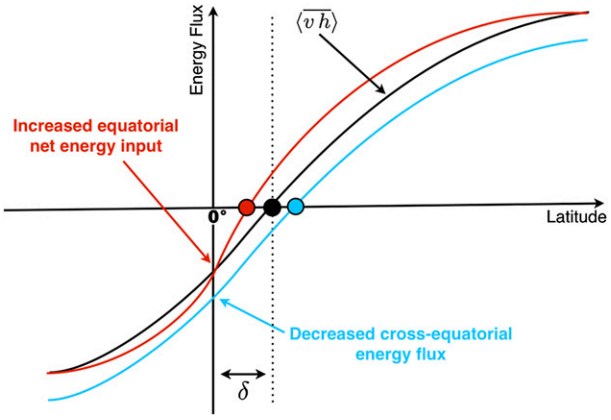

FIG. 1. Qualitative behavior of the ITCZ position (large dots) as the northward cross-equatorial atmospheric energy flux $\langle \overline{v}\overline{h} \rangle_0$ decreases (blue line) and as the net energy input to the equatorial atmosphere $\mathcal{S}_0 - \mathcal{L}_0 - \mathcal{O}_0 = \partial_y \langle \overline{v}\overline{h} \rangle_0$ increases (red line). Decreased northward energy flux at the equator shifts the zero of the energy flux and hence the ITCZ poleward. Increased energy input increases the divergence (slope) of the energy flux and shifts its zero and hence the ITCZ equatorward.

This shows that the ITCZ position, to first order in δ, is proportional to the negative of the atmospheric energy flux across the equator $\langle \overline{v}\overline{h} \rangle_0$, with the sensitivity of this dependence (the proportionality "constant," which need not be constant) determined by the net energy input to the equatorial atmosphere $\mathcal{S}_0 - \mathcal{L}_0 - \mathcal{O}_0$.[2] For Earth's annual- and zonal-mean equatorial net energy input of about 10–20 W m^{-2} (Fasullo and Trenberth 2008), it implies that the ITCZ shifts approximately 1°–2° southward for every 0.1 PW increase in northward cross-equatorial atmospheric energy transport, holding the net energy input fixed.

Equation (3) provides a first-order quantitative basis for understanding the anticorrelation between cross-equatorial energy transport and ITCZ position seen in GCM simulations (e.g., Kang et al. 2008, 2009; Frierson and Hwang 2012; Donohoe et al. 2013). Additionally, it explains how and by how much the ITCZ can shift in response to equatorial changes that may not have a signature in cross-equatorial energy transport: If the net energy input to the equatorial atmosphere in the denominator of Eq. (3) changes, the sensitivity of the ITCZ position to cross-equatorial energy transport changes, and that alone can shift the ITCZ (see Fig. 1 for an illustration). For example, the increased net energy input to the equatorial atmosphere during El Niño by itself (apart from any change in cross-equatorial energy transport) implies an equatorward shift of the ITCZ according to Eq. (3), as is in fact observed (e.g., Dai and Wigley 2000; Berry and Reeder 2014). Changes in the net energy input to the equatorial atmosphere may also explain why the ITCZ shifts as tropical cloud parameterizations are varied in GCMs (Kang et al. 2008, 2009).

The linear approximation implicit in Eq. (3) gives the exact position of the zero of the atmospheric energy flux if the energy flux varies linearly with latitude in the vicinity of the equator (as illustrated in Fig. 1). Where this is inaccurate—that is, where the energy flux varies more strongly with latitude near the equator, as it does regionally—higher-order terms in the expansion, involving higher derivatives of the atmospheric energy flux near the equator, may be needed to improve the approximation. However, in the zonal and annual mean, Eq. (3) approximates the zero of the atmospheric energy flux to within 1°–2° accuracy, according to the data provided by Fasullo and Trenberth (2008).

To connect the cross-equatorial energy transport to interhemispheric asymmetries, we integrate the energy balance [Eq. (1)] separately from the equator to the latitudes ϕ_N and ϕ_S near the northern and southern edges of the Hadley circulation where the mean meridional energy flux $\langle \overline{v}\overline{h} \rangle$ vanishes, and the total flux $\langle \overline{v}\overline{h} \rangle = \langle \overline{v}\overline{h} \rangle + \langle \overline{v'h'} \rangle$ approximately reduces to the eddy flux $\langle \overline{v'h'} \rangle$. In the present climate, this occurs near $\phi_{N,S} \approx \pm 35°$. The two integrations yield two expressions that can be combined to give the cross-equatorial atmospheric energy flux in terms of interhemispheric asymmetries in eddy energy fluxes at ϕ_S and ϕ_N and in the net atmospheric energy input between ϕ_S and ϕ_N,

$$\langle \overline{v}\overline{h} \rangle_0 \approx \{ \langle \overline{v'h'} \rangle \}_S^N - \left\{ \int_0^y (\mathcal{S} - \mathcal{L} - \mathcal{O})\, dy \right\}_S^N . \quad (4)$$

Here, the braces $\{\cdot\}_S^N$ denote the arithmetic mean of $(\cdot)$ evaluated at ϕ_N and ϕ_S. This relation is diagnostic in the sense that the location where the mean meridional energy flux vanishes is not a constant but may change with climate. For a hemispherically symmetric planet, the eddy energy flux and input integral on the right-hand side of Eq. (4) are hemispherically antisymmetric; their arithmetic means at ϕ_N and ϕ_S are zero, and so is the cross-equatorial atmospheric energy flux. Any nonzero cross-equatorial atmospheric energy flux arises from asymmetries in the eddy energy flux at $\phi_{N,S}$ and from asymmetries in the energy input to the atmosphere within the tropical latitude belt between ϕ_S and ϕ_N, for example, by asymmetries in ocean energy flux divergence. On

[2] A slightly more accurate relation is obtained if the net energy input in the denominator is not evaluated at the equator but is averaged between the equator and the ITCZ; however, given the uncertainties in the inferred net energy input, this makes little difference in Earth's atmosphere.

Earth currently, the eddy flux $\langle \overline{v'h'} \rangle$ approximately exports 0.5 PW more at the southern edge of the tropics than at the northern, giving a hemispherically asymmetric contribution [first term on the right-hand side of Eq. (4)] of about −0.25 PW (Frierson et al. 2013). By contrast, the interhemispheric asymmetry in the net energy input to the tropical belt (second term) amounts to about 0.1 PW and so is comparatively small (Fasullo and Trenberth 2008). From this perspective, an annual- and zonal-mean ITCZ in the Northern Hemisphere arises primarily because eddies transport more energy poleward in the southern than in the northern extratropics (cf. Kang et al. 2008, 2009), at least in part because the oceanic meridional overturning circulation cools the southern and warms the northern high latitudes (Fučkar et al. 2013; Marshall et al. 2013; Frierson et al. 2013). This leads to weaker pole–equator temperature gradients and weaker eddy energy fluxes in the Northern Hemisphere and ultimately to a northward displaced ITCZ. However, these inferences are uncertain, because both oceanic and atmospheric energy fluxes and the net energy input to the atmosphere within the tropical belt are uncertain, with standard errors in meridional energy fluxes of at least ±0.2 PW (Ganachaud and Wunsch 2000; Mayer and Haimberger 2012).

Before relating interhemispheric asymmetries in energy fluxes to those in surface temperatures through a series of closure approximations, we illustrate and test the energetic constraints on the ITCZ position with GCM simulations.

3. GCM simulations

We use an idealized moist GCM to be able to test the validity of the theoretical Eqs. (3) and (4) over a wider range of climates than those of Earth's recent past and proximate future. This allows us to delineate the range of validity of the expressions more clearly than would be possible by analyzing observations or simulating climate changes with a comprehensive GCM. With the idealized GCM, we can investigate separately the effects of tropical energy input changes and cross-equatorial energy flux changes, effects that usually occur together during ENSO or global warming. Our GCM is that of O'Gorman and Schneider (2008), which is similar to that used in Frierson et al. (2006) and Frierson (2007). The GCM uses a two-stream radiation scheme without clouds or aerosols, and the lower boundary consists of a slab ocean. We explore two different energy budget perturbations, one global and one tropical: (i) we vary the longwave optical depth of the atmosphere globally, leading to global temperature changes, with global-mean surface temperatures spanning the large range from 275 to 315 K, and (ii) we vary an imposed ocean energy flux convergence in a thin band around the equator, leading to primarily tropical temperature changes, with tropical surface temperatures spanning 303–308 K. (We have verified that this zonally symmetric surface heating has the same effect in the zonal mean as a zonally more localized surface heating with the same zonal mean, which would be more representative of El Niño.) For the atmospheric circulation to be hemispherically asymmetric, we also impose a hemispherically antisymmetric ocean energy uptake/release $\mathcal{O}$ outside 30°N/S, which cools the southern and warms the Northern Hemisphere, in a similar way as in Kang et al. (2008, 2009). This may represent, for example, energy transport associated with an oceanic meridional overturning circulation or interhemispheric differences in surface albedo such as those due to differences in ice cover. The resulting poleward atmospheric energy fluxes are stronger in the southern than in the Northern Hemisphere and lead to an ITCZ north of the equator, as on Earth. Details of the simulations are given in appendix A.

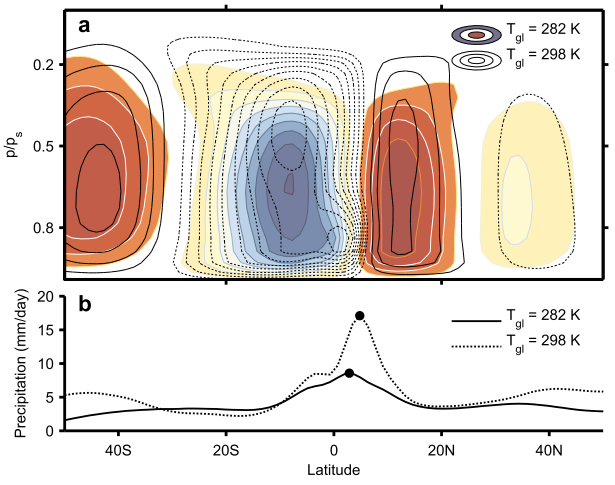

FIG. 2. (a) Mass flux streamfunction and (b) precipitation for global-mean surface temperatures T_{gl} = 282 K and T_{gl} = 298 K in the global warming scenario. The contour interval in (a) is 1.6×10^{10} kg s^{-1}. Red/solid contours show northward mass transport, and blue/dashed contours show southward mass transport. The maximum and minimum values of the streamfunctions are 7.8×10^{10} kg s^{-1} and -14.5×10^{10} kg s^{-1} at T_{gl} = 282 K and 7.1×10^{10} kg s^{-1} and -15.8×10^{10} kg s^{-1} at T_{gl} = 298 K. The black dots in (b) mark the precipitation maximum. The ITCZ generally is farther poleward in warmer climates, and the maximum precipitation is strengthened. In addition, the Hadley cells expand and the tropopause height increases. The zero of the mass flux streamfunction moves poleward with global-mean surface temperature but remains poleward of the precipitation maximum.

a. Global warming

The contours in Fig. 2a show typical mass flux streamfunctions for a cold and a warm case in the global warming

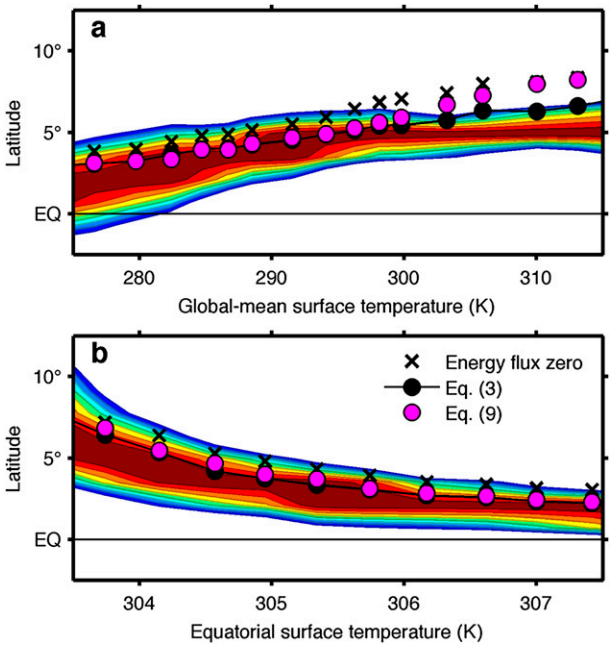

FIG. 3. ITCZ position in GCM simulations under (a) global and (b) tropical warming. Colors show precipitation normalized by its global maximum, with contours from 0.9 to 1.0. Black crosses indicate where the moist static energy flux is zero. Black dots show the ITCZ latitude δ calculated from Eq. (3). Magenta dots show the approximate ITCZ latitude δ calculated from Eq. (8). The horizontal axes are (a) global-mean surface temperature and (b) equatorial surface temperature. The ITCZ shifts are qualitatively different in the two series of simulations: Under global warming, the ITCZ shifts are primarily caused by hemispherically asymmetric changes in extratropical latent energy fluxes and associated changes in cross-equatorial energy flux (cf. blue line in Fig. 1). Under tropical warming, the ITCZ shifts are primarily caused by changes to the net energy input to the equatorial atmosphere (cf. red line in Fig. 1).

scenario. In the warmer climate, the region of maximum low-level upward mass flux and the zero contour of the mass flux streamfunction are located farther away from the equator. This accompanies an increase in tropopause height and Hadley circulation width (cf. Schneider et al. 2010; O'Gorman et al. 2011; Levine and Schneider 2011). At the same time, the precipitation maximum (Fig. 2b) lies farther away from the equator in the warmer climate, as does the collocated maximum of the low-level upward mass flux. The precipitation maximum is also strengthened in the warmer climate, primarily because of the increased near-surface specific humidity in the tropics.

Generally, as the longwave optical depth and global-mean surface temperature increase, the ITCZ and its tropical precipitation maximum shift monotonically away from the equator (Fig. 3a). Our estimate in Eq. (3) of the ITCZ position captures this shift to within $\lesssim 2°$ (Fig. 3a, black dots). If the cross-equatorial energy flux $\langle \overline{vh} \rangle_0$ is related to interhemispheric asymmetries as in Eq. (4), the resulting estimate of the ITCZ position is essentially indistinguishable from that shown in Fig. 3a. The larger errors in the warmer climates arise in part because the ITCZ as defined by the precipitation maximum and the zero of the atmospheric energy flux (Fig. 3a, crosses) begin to diverge and are up to 2° apart in the warmest climates.

In the global warming simulations, changes in δ are primarily associated with hemispherically asymmetric changes in extratropical eddy energy fluxes (Fig. 5a). Changes in the net energy input to the equatorial atmosphere by themselves would imply an equatorward shift of the ITCZ as the climate warms (Fig. 6a). Their effect (2° equatorward ITCZ shift over the range of simulations) is overcompensated by the effect of the energy flux changes (7° poleward shift). In our simulations, the net energy input to the equatorial atmosphere increases with increasing global-mean surface temperature primarily because the equatorial top-of-atmosphere outgoing longwave radiation decreases as the temperature increases. This is because the atmosphere exports more energy from the tropics to the extratropics in warmer climates, thus increasing the radiative imbalance at the top of the atmosphere at the equator. If changes in δ are regressed onto changes in the cross-equatorial atmospheric energy flux $\langle \overline{vh} \rangle_0$ alone, disregarding that the energy input to the equatorial atmosphere also varies, we find that δ increases by 3°–4° for every 1-PW reduction in $\langle \overline{vh} \rangle_0$, quantitatively consistent with studies that regress the location of maximum precipitation directly on the cross-equatorial energy transport (Donohoe et al. 2013, 2014). However, this overemphasizes the role of the cross-equatorial energy flux, because the energy input to the equatorial atmosphere varies simultaneously. If changes in δ are regressed onto changes in both the cross-equatorial atmospheric energy flux and the net energy input to the equatorial atmosphere, δ increases by 4°–6° for every 1-PW reduction in $\langle \overline{vh} \rangle_0$, holding the energy input to the equatorial atmosphere fixed.

Decomposing the cross-equatorial energy flux into components as in Eq. (4) shows that the principal reason for the monotonic poleward shift of the ITCZ under global warming lies in a strengthening of extratropical latent energy fluxes and their hemispherically asymmetric component, which overcompensate nonmonotonic changes in extratropical dry static energy fluxes (Fig. 5a). This is in agreement with earlier studies that identified the latent energy flux as the main driver of ITCZ shifts in CO_2-doubling simulations in idealized setups (e.g., Hwang and Frierson 2010; Frierson and Hwang 2012). It is also consistent with the notion that latent energy fluxes dominate the poleward energy flux in warm climates (Pierrehumbert 2002; Caballero and Langen 2005;

O'Gorman and Schneider 2008; Caballero and Hanley 2012), with preexisting asymmetries in latent energy fluxes amplifying as the climate warms (Held and Soden 2006).

The response of the ITCZ location to increases of the longwave optical depth likely depends on the strength of the imposed hemispherically antisymmetric ocean energy uptake/release $\mathcal{O}$ in midlatitudes. A stronger preexisting antisymmetry in ocean energy uptake/release implies a stronger response of the eddy moist static energy flux term in Eq. (4) because of the Clausius–Clapeyron nonlinearity that governs latent energy flux changes (e.g., Held and Soden 2006). As a consequence, the response of the ITCZ location to increased longwave optical depth may be nonmonotonic for some strengths of the antisymmetric ocean energy uptake/release.

b. Tropical warming

The contours in Fig. 4a show typical mass flux streamfunctions for a cold and a warm case in the tropical warming scenario. The region of maximum low-level upward mass flux and the zero contour of the mass flux streamfunction are located closer to the equator in climates with higher equatorial surface temperatures. At the same time, the Hadley circulation is narrower and stronger, resembling qualitatively (albeit not quantitatively) El Niño conditions on Earth (Seager et al. 2003). The precipitation maximum (Fig. 4b) is located closer to the equator. The strengthened maximum precipitation in the case with a warmer equatorial surface arises because the mass flux is strengthened and the near-surface specific humidity in the tropics is increased.

Generally, as the imposed ocean energy flux convergence at the equator and with it tropical surface temperatures increase, the ITCZ and its tropical precipitation maximum shift toward the equator (Fig. 3b). Our estimate in Eq. (3) of the ITCZ position again captures this shift accurately, to within $\lesssim 2°$ (Fig. 3b, black dots). As for the global warming simulations, if the cross-equatorial energy flux $\langle \overline{vh} \rangle_0$ is related to interhemispheric asymmetries as in Eq. (4), the resulting estimate of the ITCZ position remains essentially indistinguishable from that shown in Fig. 3b. In contrast to the global warming simulations, however, changes in δ in the tropical warming simulations are primarily associated with changes in the net energy input to the equatorial atmosphere. The equatorial net energy input increases monotonically and strongly (Fig. 6b); however, the cross-equatorial energy flux remains nearly unchanged (Fig. 5b).

Increasing the width of the tropical forcing does not change the response qualitatively as long at the impact on moist static energy fluxes associated with extratropical eddies remains small. This is consistent with the linear approximation implicit in Eq. (3) because the denominator only depends on the amplitude of the net energy input at the equator.

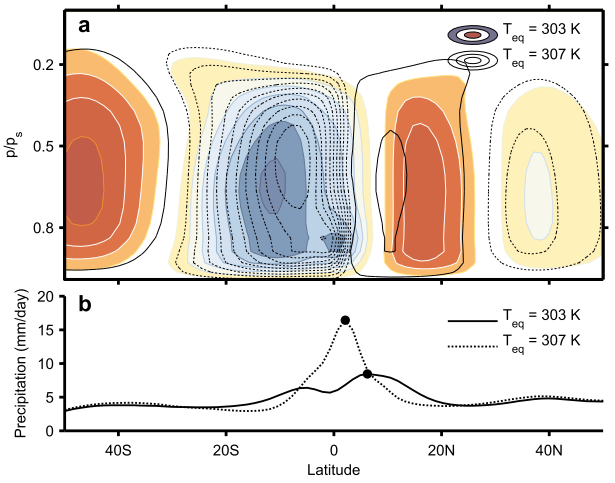

FIG. 4. (a) Mass flux streamfunction and (b) precipitation for equatorial surface temperatures $T_{eq} = 303$ K and $T_{eq} = 307$ K in the tropical warming scenario. Colors and contours are as in Fig. 2. The maximum and minimum values of the streamfunctions are 6.9×10^{10} kg s^{-1} and -11.5×10^{10} kg s^{-1} at $T_{eq} = 303$ K and 8.8×10^{10} kg s^{-1} and -17.8×10^{10} kg s^{-1} at $T_{eq} = 307$ K. The black dots in (b) mark the precipitation maximum. The ITCZ is generally located closer to the equator in simulations with higher equatorial surface temperatures, and the maximum precipitation is strengthened. In addition, the Hadley cells contract. The zero of the mass flux streamfunction moves equatorward as equatorial surface temperatures increase, but it remains poleward of the precipitation maximum.

c. Implications

The simulations illustrate how cross-equatorial energy transport and the net energy input to the equatorial atmosphere act together to determine the ITCZ position. They demonstrate that changes in the ITCZ position do not need to be correlated with changes in cross-equatorial energy transport but can be associated with changes in equatorial net energy input alone.

In reality, most changes in ITCZ position likely are a superposition of changes in tropical energy input and cross-equatorial energy transport. Such changes can be caused by a variety of processes, from changes in cloud albedo and aerosol loading to changes in ocean upwelling. For example, an increased equatorial shortwave albedo (everything else fixed) reduces the net incoming shortwave radiation $\mathcal{S}_0$ and makes the ITCZ position more sensitive to a given cross-equatorial energy transport, leading to a poleward shift of the ITCZ. Similarly, weakened upwelling and energy uptake $\mathcal{O}_0$ by the equatorial oceans leads to an equatorward shift of the ITCZ. Such tropical changes can act together or in concert with

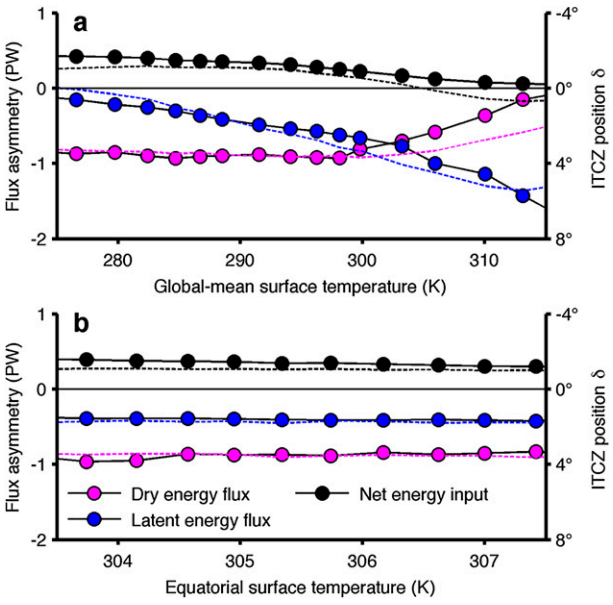

FIG. 5. Interhemispheric asymmetries in energy fluxes in GCM simulations under (a) global warming and (b) tropical warming. The interhemispheric asymmetries are measured by the arithmetic mean of the fluxes at the subtropical latitude where the mean moist static energy flux $\langle \overline{v}\overline{h} \rangle$ in each hemisphere is zero. Plotting symbols and solid lines show the flux asymmetries and the negative energy input into the tropical atmosphere in the GCM simulations. Dashed lines show the respective approximations [Eqs. (5) and (6)]. The right axis shows the implied ITCZ position when the denominator in Eq. (3) is taken from a reference climate with a global-mean surface temperature of 288 K and an equatorial surface temperature of 304 K. Under global warming, the latent energy fluxes experience the largest changes, primarily because of large changes in subtropical saturation specific humidity [cf. Eq. (5)]. Under tropical warming, hemispherically asymmetric changes in energy fluxes are small.

changes in extratropical eddy energy fluxes to lead to complex changes in the ITCZ position.

4. Closure approximations

While the expressions for the ITCZ position in terms of energy fluxes are relatively accurate, it is desirable to relate the ITCZ position to quantities that are more easily measured or inferred, in particular for climates of the past. To do so, we relate the relevant energy fluxes through a series of closure approximations to near-surface temperatures.

a. Atmospheric eddy energy fluxes

The eddy energy flux $\langle \overline{v'h'} \rangle = \langle \overline{v's'} \rangle + \langle \overline{v'l'} \rangle$ at the edges of the tropical belt is a mediator between low and high latitudes and communicates extratropical changes to the tropics and tropical changes to the extratropics. The simplest closure approximation of this vertically integrated flux is a diffusive mixing length closure (e.g., Frierson 2007; Kang et al. 2009), which is best justifiable for conserved quantities on scales larger than typical eddy length scales. However, closure approximations for fluxes of latent energy (water vapor) must take into account that moist air parcels from the subtropical boundary layer are transported upward and poleward, losing moisture along the way through cooling, condensation, and precipitation. The vertical structure of the flux must be considered, which can lead to a nonlocal dependence of water vapor fluxes, for example, on a subtropical specific humidity (Pierrehumbert 2002; Caballero and Langen 2005; O'Gorman and Schneider 2006; Pierrehumbert et al. 2007; O'Gorman and Schneider 2008; O'Gorman et al. 2011; Caballero and Hanley 2012).

We use a diffusive closure for the vertically integrated moist static energy flux $\langle \overline{v'h'} \rangle$, which approximates the vertically integrated dry static energy flux $\langle \overline{v's'} \rangle$ in terms of near-surface temperature gradients and the vertically integrated latent energy flux $\langle \overline{v'l'} \rangle$ by taking into account the strong vertical structure of specific humidity through diffusion of moisture along dry isentropes (see appendix B). The approximate eddy moist static energy flux at the edges of the tropics is given by

$$\langle \overline{v'h'} \rangle \approx \langle \overline{v's'} \rangle (1 + \beta q_s) \approx \pm \alpha v_e \Delta T (1 + \beta q_s). \quad (5)$$

The coefficient α includes the relevant physical constants and depends on the location of the storm track. The velocity v_e is a typical eddy velocity, and $\Delta T = T_{70°\mathrm{N,S}} - T_{20°\mathrm{N,S}}$ is the pole to subtropics temperature difference evaluated at the top of the boundary layer between 70° and 20° latitude in each hemisphere (see appendix B). Annual-mean reanalysis data for Earth's current atmosphere indicate $\alpha \approx 2.3 \times 10^5\,\mathrm{J\,K^{-1}\,m^{-2}}$ in the Northern Hemisphere and in the Southern Hemisphere. The eddy velocity v_e varies in the Northern Hemisphere between $10\,\mathrm{m\,s^{-1}}$ in winter and $6.5\,\mathrm{m\,s^{-1}}$ in summer and in the Southern Hemisphere between $9.5\,\mathrm{m\,s^{-1}}$ in winter and $8\,\mathrm{m\,s^{-1}}$ in summer. The temperature difference ΔT between ±70° and ±20° latitude varies in the Northern Hemisphere between 32 K in winter and 18 K in summer and in the Southern Hemisphere between 32.5 K in winter and 29.5 K in summer (Uppala et al. 2005). This formulation also captures the contribution of stationary eddies to the dry static energy flux, although, unlike for transient eddies, it is more difficult to justify using diffusive closures for stationary eddies.

In our simulations, where there are only transient eddies, Eq. (5) captures the variations of the interhemispheric asymmetry in the dry static energy fluxes [first term in Eq. (5)] to within 15% in climates with global-mean surface temperatures $\lesssim$305 K (Fig. 5). We relate the latent energy flux, directed poleward and upward

approximately along isentropes from the subtropics to the extratropics (e.g., Galewsky et al. 2005), to the dry static energy flux $\langle\overline{v's'}\rangle$ by using the slope of near-surface isentropes averaged over the extratropics and the saturation specific humidity q_s evaluated in the subtropics [see O'Gorman and Schneider (2008) and appendix B]. The resulting approximation of the latent energy flux is the dry static energy flux multiplied by the factor βq_s, where β depends on the subtropical relative humidity, near-surface temperature, and extratropical near-surface static stability. For Earth's current atmosphere, reanalysis data indicate $\beta q_s \approx 0.8$ in the Northern Hemisphere and 0.9 in the Southern Hemisphere in the annual mean (Uppala et al. 2005), showing that dry static and latent energy fluxes are of similar importance in both hemispheres. In our simulations, this formulation captures the variations of the interhemispheric asymmetry in the latent energy fluxes to within 30% for climates with global-mean surface temperatures $\gtrsim$285 K (Fig. 5).

For all simulations presented, this closure for eddy moist static energy fluxes is essentially indistinguishable from diffusing moist static energy directly: that is, approximating $\langle\overline{v'h'}\rangle$ in terms of the near-surface moist static energy gradient. The main difference lies in the functional dependence of β on other quantities (see appendix B). However, the choice of closure does not affect our conclusions in what follows.

b. Asymmetric energy input to tropical belt

In addition to hemispherically asymmetric eddy energy fluxes at the edges of the tropical belt, the hemispherically asymmetric net energy input to the atmosphere in the tropical belt [second term on right-hand side of Eq. (4)] also contributes to interhemispheric asymmetries and hence to cross-equatorial energy transport. In our and other simulations and in observational data (Uppala et al. 2005; Fasullo and Trenberth 2008), however, the interhemispheric differences in eddy energy fluxes at the edges of the tropical belt contribute at least 50% to the cross-equatorial energy flux. In the simulations, the contribution of the asymmetric net energy input to the tropical belt is smaller, with all of it being attributable to asymmetries in the outgoing longwave radiation (Fig. 5). We therefore approximate the net energy input to the atmosphere in the tropical belt as

$$\left\{\int_0^y (\mathcal{S}-\mathcal{L}-\mathcal{O})\,dy\right\}_S^N \approx -\gamma(T_{20^\circ\mathrm{N}}-T_{20^\circ\mathrm{S}}). \quad (6)$$

Here, $\gamma \approx 2.8\times10^6\,\mathrm{W\,K^{-1}\,m^{-1}}$ for the simulations, and $\gamma \approx 1.7\times10^6\,\mathrm{W\,K^{-1}\,m^{-1}}$ for Earth's atmosphere (Fasullo and Trenberth 2008). Asymmetries in ocean energy uptake $\mathcal{O}$ between the hemispheres are important for Earth's atmosphere and likely account for much of the difference in γ to the simulations; hemispheric asymmetries in net shortwave radiation in the tropics may also contribute, although they are small when averaged over the entire hemispheres (Marshall et al. 2013; Voigt et al. 2013). In our simulations, this formulation introduces errors less than 30% for global-mean temperatures between 280 and 300 K, with larger errors in warmer climates (see Fig. 5).

The overall error in the cross-equatorial energy transport introduced by the various approximations does not exceed 30% over the range of simulations presented here. This is a relatively good approximation given that the interhemispheric asymmetry is a small difference between the large eddy fluxes in each hemisphere (see appendix B) and given that global-mean surface temperatures vary by 40 K over the range of simulations.

c. Equatorial energy input to the atmosphere

For the purpose of this paper, we treat the net incoming shortwave radiation at the equator $\mathcal{S}_0$ and the equatorial ocean energy uptake $\mathcal{O}_0$ as external parameters, without attempting to relate them to the climate state. In reality, of course, both are related to the climate state, through the shortwave albedo (e.g., cloudiness) and ocean energy flux, which is intimately coupled to the atmospheric circulation and its energy flux (Klinger and Marotzke 2000; Held 2001). This leaves us to relate the outgoing longwave radiation at the equator $\mathcal{L}_0$ to the climate state and specifically the equatorial surface temperature T_0. We do so by relating the surface temperature to the temperature at the emission height H_0 by $T_0 - \Gamma_0 H_0$, where Γ_0 is the vertically averaged (moist adiabatic) lapse rate at the equator ($\Gamma_0 \approx 5.3\,\mathrm{K\,km^{-1}}$ in Earth's present climate). Linearizing the Stefan–Boltzmann law around a reference temperature $\check{T}$ then gives, for the outgoing longwave radiation at the equator,

$$\mathcal{L}_0 \approx \sigma_b \check{T}^4 + 4\sigma_b \check{T}^3(T_0 - \Gamma_0 H_0 - \check{T}), \quad (7)$$

with the Stefan–Boltzmann constant σ_b. The emission height at the equator varies with the concentration and distribution of infrared absorbers. In Earth's present climate, $H_0 \approx 8$ km is a good approximation (Uppala et al. 2005), but H_0 increases as the concentration of greenhouse gases increases. This gives an excellent approximation of the equatorial outgoing longwave radiation $\mathcal{L}_0$, with errors of less than 10% across our simulations if variations in Γ_0 and H_0 are taken into account but $\check{T} = 250$ K is taken as fixed (Fig. 6).

d. ITCZ position

Combining the above approximations to reexpress the ITCZ position in Eq. (3) gives

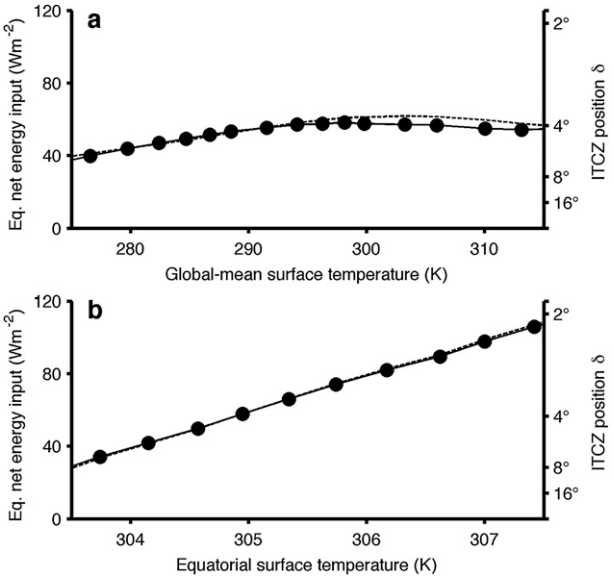

FIG. 6. Net energy input to the atmosphere at the equator in GCM simulations under (a) global and (b) tropical warming. Dots and solid lines show the GCM results; dashed lines show approximations in which the outgoing longwave radiation is approximated [Eq. (7)]. The right axis shows the implied ITCZ position when the numerator in Eq. (3) is taken from a reference climate with a global-mean surface temperature of 288 K and an equatorial surface temperature of 304 K. The reciprocal of the net energy input at the equator is a measure of the sensitivity of the ITCZ position to interhemispheric asymmetries in energy fluxes. Under global warming, the changes in the net energy input by themselves would imply an equatorward shift of the ITCZ in colder climates and little change in warmer climates. In fact, however, the ITCZ shifts poleward (Fig. 3a), implying changed interhemispheric asymmetries in energy fluxes (Fig. 5a) dominate the ITCZ shift. Under tropical warming, the changes in the net energy input imply an equatorward shift of the ITCZ, which in fact occurs (Fig. 3b).

$$\delta \approx -\frac{1}{a}\frac{\{\alpha v_e \Delta T(1+\beta q_s)\}_S^N + \gamma(T_{20^\circ\mathrm{N}} - T_{20^\circ\mathrm{S}})}{\mathcal{S}_0 - \sigma_b \check{T}^4 - 4\sigma_b \check{T}^3(T_0 - \Gamma_0 H_0 - \check{T}) - \mathcal{O}_0}. \tag{8}$$

Estimating the different terms from annually and zonally averaged reanalysis data (Uppala et al. 2005) and using $20\,\mathrm{W\,m^{-2}}$ for the net energy input in the denominator (Fasullo and Trenberth 2008) gives $\delta = 6^\circ$ for the present climate, consistent with observations. Equation (8) shows how an expression for the ITCZ position involving energy fluxes can be converted into one involving surface temperatures and, in particular, hemispheric surface temperature contrasts, among other quantities. It makes explicit how perspectives focusing on energy fluxes (e.g., Kang et al. 2008, 2009) and those focusing on surface temperatures (e.g., Cvijanovic and Chiang 2013) can be reconciled.

In our simulations, Eq. (8) captures much of the overall shift of the ITCZ. Under global warming, it captures the poleward shift well for global-mean surface temperatures between 280 and 300 K (Fig. 3a); however, the poleward shift for warmer climates is not estimated accurately because interhemispheric asymmetries in dry static and latent energy fluxes are not estimated accurately (Fig. 5a). Under tropical warming, it captures the equatorward shift of the ITCZ over the entire range of simulations (Fig. 3b).

Neglecting interhemispheric differences between all components except near-surface temperatures shows why the ITCZ is generally located in the warmer hemisphere,

$$\delta \propto \frac{(T_{70^\circ\mathrm{N}} - T_{70^\circ\mathrm{S}}) - \epsilon(T_{20^\circ\mathrm{N}} - T_{20^\circ\mathrm{S}})}{\mathcal{S}_0 - \mathcal{L}_0 - \mathcal{O}_0}. \tag{9}$$

Here, $\epsilon \approx 2$ depends only on the parameters multiplying the temperatures in Eq. (8). Because in the annual and zonal mean, temperature contrasts between high latitudes of the Northern and Southern Hemispheres (about 7 K) are generally larger than temperature contrasts between the subtropics (about 2 K), the numerator in Eq. (9) is positive for Earth's present climate. This leads to a mean ITCZ position $\delta > 0$ in the Northern Hemisphere. It also explains why the ITCZ position is correlated with interhemispheric temperature differences (Friedman et al. 2013), provided the subtropical temperatures in the Northern and Southern Hemispheres are taken as approximately equal.

5. Conclusions and discussion

We have shown that the ITCZ position in the zonal mean is approximately determined by two factors: the cross-equatorial energy transport in the atmosphere and the net energy input to the equatorial atmosphere [Eq. (3)]. Atmospheric energy fluxes are generally directed away from the ITCZ in the zonal mean, implying that the ITCZ is located close to a zero of the atmospheric meridional energy flux, as has been previously demonstrated (e.g., Kang et al. 2008, 2009). For an ITCZ not too far from the equator, so that the atmospheric energy flux can be approximated as varying linearly with latitude between the equator and the ITCZ, it then follows that a northward energy flux across the equator implies an ITCZ in the Southern Hemisphere and that a southward energy flux across the equator implies an ITCZ in the Northern Hemisphere. How far from the equator the ITCZ is located is controlled by the divergence of the atmospheric energy flux at the equator or by the slope of the energy flux as a function of latitude

(Fig. 1). Because this is equal to the net energy input to the equatorial atmosphere (neglecting energy storage in the atmosphere), it is the net energy input to the equatorial atmosphere that controls the sensitivity of the ITCZ position to cross-equatorial energy transport. The hemispheric energy balance, in turn, shows how the cross-equatorial energy transport is related to interhemispheric contrasts in extratropical eddy energy fluxes and in the tropical energy input to the atmosphere [Eq. (4)].

Relating extratropical eddy energy fluxes and the tropical net energy input to the atmosphere through a series of closure approximations to surface temperatures, among other factors, we have shown how ITCZ variations associated with energetic changes can be related to temperature changes, both in the tropics and in the interhemispheric temperature contrast [Eqs. (8) and (9)]. This reconciles perspectives on the ITCZ position that have focused on energy fluxes with those that have focused on surface temperatures and interhemispheric temperature contrasts. It shows that these perspectives are not mutually contradictory but are in fact compatible with each other and complementary.

Our theory and simulations allow us to offer unified interpretations of seemingly disparate previous results. Paleoclimatological evidence and more recent observations and simulations show that the ITCZ has shifted in the past and suggest that the ITCZ can shift with variations in atmospheric greenhouse gas concentrations, aerosol loadings, and El Niño (Dai and Wigley 2000; Sachs et al. 2009; Hwang and Frierson 2010; Hwang et al. 2013; Berry and Reeder 2014). The anticorrelation between ITCZ position and cross-equatorial energy transport has been noted in many previous studies. On the basis of that anticorrelation, however, it has been suggested that for some of the observed and inferred ITCZ shifts—for example, during the Little Ice Age—large changes in cross-equatorial energy transport would be necessary (Donohoe et al. 2013). Our results instead suggest that smaller changes in cross-equatorial energy transport may account for the observed or inferred shifts when changes in the net energy input to the equatorial atmosphere are also considered. In other words, the correlation coefficient between the ITCZ position and the cross-equatorial atmospheric energy transport (or the interhemispheric temperature contrast) depends on climate. For example, in our global warming simulations, the ITCZ position depends approximately linearly on the cross-equatorial atmospheric energy transport, moving 3°–4° poleward for every 1-PW reduction in the energy transport, quantitatively consistent with previous studies (e.g., Donohoe et al. 2013). However, this overemphasizes the importance of the cross-equatorial energy flux and conceals the role of the equatorial net energy input to the atmosphere, which varies at the same time. If the net energy input to the atmosphere is kept fixed, the ITCZ position moves 4°–6° poleward for every 1-PW reduction in the energy transport, quantitatively consistent with our first-order estimate Eq. (3).

Previous modeling studies with aquaplanet GCMs with slab oceans have shown that the ITCZ is typically located in the warmer hemisphere because the atmosphere transports energy across the equator into the colder hemisphere (Broccoli et al. 2006; Yoshimori and Broccoli 2008; Kang et al. 2008, 2009; Frierson and Hwang 2012). In this picture, high-latitude changes (e.g., in ice cover) are communicated to the tropics by large-scale extratropical eddies and ocean circulations. Differential warming in one hemisphere, even far from the equator, can then drive ITCZ shifts toward that hemisphere (Chiang et al. 2003; Donohoe et al. 2013; Cvijanovic and Chiang 2013). Our approximate quantitative expression [Eq. (8)] for the ITCZ position shows how interhemispheric temperature differences relate to the ITCZ position: namely, primarily through interhemispheric differences in extratropical meridional temperature contrasts.

Because the ITCZ is not only controlled by interhemispheric asymmetries in energy fluxes that lead to cross-equatorial energy transport but also by the net energy input to the equatorial atmosphere, the ITCZ can shift even without cross-equatorial energy transport changes: for example, when there is reduced equatorial ocean energy uptake, such as during El Niño. This shows that also tropical processes alone (e.g., changes in cloud albedo or energy uptake by the equatorial oceans) can lead to ITCZ shifts. Thus, to understand future ITCZ shifts, it is important to understand not only changes in cross-equatorial energy transport, which can be remotely triggered, but also tropical changes in equatorial upwelling, El Niño, and the equatorial cloud and aerosol distributions, as they all enter the equatorial energy balance.

We have approached the question of what sets the position of the ITCZ from an energetic perspective, leading to results that depend on, among other factors, near-surface temperatures. This leaves open the question of what determines the temperatures. Answering that question requires consideration of the angular momentum balance of the atmosphere and how it controls the circulations that accomplish the atmospheric energy transport (e.g., Walker and Schneider 2006; Schneider 2006; Schneider et al. 2010; Levine and Schneider 2011). Additionally, the ITCZ defined by the precipitation maximum is not always collocated with the zero of the atmospheric energy flux, because the maximum upward mass flux and mean precipitation maximum are

determined by the meridional derivative of the mass flux streamfunction and not necessarily by where the streamfunction (or the energy flux) vanish (Donohoe et al. 2013, 2014). A completely closed theory of the tropical precipitation maximum therefore would require understanding both the angular momentum and energy balances of the tropical troposphere. Additionally, for a theory that can also be applied to seasonal variations, it will be important to have a theory of seasonal ocean energy storage and release. Particularly for monsoon regions, it is questionable whether energy fluxes alone will give a sufficiently accurate picture of ITCZ variations (Chiang and Friedman 2012). Even when they do, it may become necessary to go beyond the linear approximations of energy fluxes on which we focused in this paper.

Acknowledgments. We thank Gerald Haug for stimulating discussions during the course of this research and Simona Bordoni and Robert Wills for helpful comments on drafts of the paper. Comments by two anonymous reviewers greatly helped to improve the quality of this paper. This work was supported by NSF Grants AGS-1019211, AGS-1049201, and AGS-1003614. Idealized GCM simulations were performed on Caltech's Division of Geological and Planetary Science CITerra computing cluster.

APPENDIX A

Description of GCM and Simulations

The GCM has a simplified representation of the hydrological cycle and radiative transfer (Frierson et al. 2006; O'Gorman and Schneider 2008). It only takes into account the liquid–vapor phase transition, it has no ice phase, and the latent heat of evaporation is fixed at $L_v = 2.5 \times 10^6\,\mathrm{J\,kg^{-1}}$. It uses a two-stream gray radiation scheme with prescribed and time-invariant optical opacity profiles.

The top-of-atmosphere insolation is imposed as an approximate annual mean,

$$\mathcal{S} = \frac{S_0}{4}\left\{1 + \frac{\Delta_s}{4}(1 - 3\sin^2\phi)\right\}. \tag{A1}$$

Here, $S_0 = 1360\,\mathrm{W\,m^{-2}}$ is the solar constant, and $\Delta_s = 1.2$ is a nondimensional measure of the insolation gradient. The shortwave radiative flux is attenuated going downward, with increasing vertical coordinate $\sigma = p/p_s$ (pressure p normalized by surface pressure p_s) by an exponential factor $\exp(-\tau_s\sigma^2)$, where $\tau_s = 0.22$ is the shortwave optical thickness of the atmosphere. This represents roughly the absorption of shortwave radiation by atmospheric water vapor. However, dynamic radiative water vapor feedback or cloud feedbacks are not taken into account.

Longwave radiation is absorbed by an idealized absorber with a mixture of characteristics of a well-mixed greenhouse gas and water vapor. It has an optical depth $\tau = \eta\tau_{\mathrm{ref}}(\phi)$, where η is a rescaling factor that is varied in the global warming simulations to rescale the reference optical depth,

$$\tau_{\mathrm{ref}} = \{f_l\sigma + (1 - f_l)\sigma^4\}\{\tau_e + (\tau_p - \tau_e)\sin^2\phi\}. \tag{A2}$$

Here, $f_l = 0.2$ measures the fraction of the absorber whose optical depth increases with σ (i.e., an approximately well-mixed absorber), $(1 - f_l)$ is the fraction of the water vapor-like absorber, $\tau_e = 7.2$ is the longwave optical depth at the equator, and $\tau_p = 1.8$ is the longwave optical depth at the poles.

The lower boundary is a slab ocean mixed layer with uniform depth $d = 1$ m and with a uniform and constant albedo of 0.3. The surface mixed layer energy budget is given by

$$\rho_0 c_0 d\partial_t T_{\mathrm{sfc}} = \mathcal{S}_{\mathrm{sfc}} - \mathcal{L}_{\mathrm{sfc}} - \mathcal{E} - \mathcal{H} - \mathcal{O}, \tag{A3}$$

where ρ_0 is the surface water density, c_0 is the surface water heat capacity, T_{sfc} is the surface temperature, $\mathcal{S}_{\mathrm{sfc}}$ is the net downwelling shortwave radiation at the surface, $\mathcal{L}_{\mathrm{sfc}}$ is the net upwelling longwave radiation at the surface, $\mathcal{E}$ is the latent heat flux due to surface evaporation, $\mathcal{H}$ is the sensible heat flux, and $\mathcal{O}$ is the ocean energy flux divergence. The surface fluxes $\mathcal{E}$ and $\mathcal{H}$ are represented by standard bulk aerodynamic formulas.

We impose a zonally symmetric and time-independent ocean energy flux divergence (Fig. A1),

$$\mathcal{O} = \hat{O}_s\cos(\phi)^{-1}\left(1 - \frac{\phi^2}{\delta\phi_s^2}\right)\exp\left[-\frac{\phi^2}{2\delta\phi_s^2}\right] \tag{A4a}$$

$$+ \hat{O}_a\left\{\exp\left[-\frac{(\phi - \phi_{\mathrm{SH}})^2}{2\delta\phi_a^2}\right] - \exp\left[-\frac{(\phi - \phi_{\mathrm{NH}})^2}{2\delta\phi_a^2}\right]\right\} \tag{A4b}$$

$$+ \hat{O}_t\exp\left[-\frac{\phi^2}{2\delta\phi_t^2}\right]. \tag{A4c}$$

Here, $\hat{O}_s$ is the amplitude of the hemispherically symmetric ocean energy flux divergence and $\delta\phi_s = 11.3°$ (standard deviation of Gaussian) is a measure of its width around the equator. The hemispherically antisymmetric energy flux divergence with amplitude $\hat{O}_a$ is used to drive the ITCZ off the equator, with $\phi_{\mathrm{NH}} = 60°$,

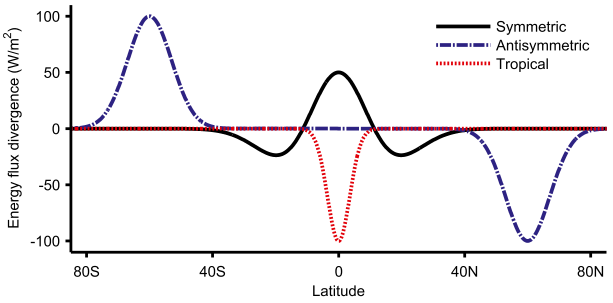

FIG. A1. The different components of the ocean energy flux divergence used in the idealized GCM experiments. The solid black line shows the symmetric ocean energy flux divergence with amplitude 50 W m^{-2} given by the term in Eq. (A4a). It is used in the tropical warming experiments. The dashed–dotted blue line shows the antisymmetric ocean energy flux divergence with amplitude 100 W m^{-2} that is used to drive the ITCZ off the equator in all experiments. Its functional form is given by the term in Eq. (A4b). The dashed red line shows the tropical ocean energy flux divergence with amplitude -100 W m^{-2} that is used in the tropical warming simulations. Its functional form is given by the term in Eq. (A4c).

$\phi_{\mathrm{SH}} = -\phi_{\mathrm{NH}}$, $\delta\phi_a = 7°$, and $\hat{O}_a = 100\,\mathrm{W\,m^{-2}}$ in all simulations. It represents an interhemispheric asymmetry in the high-latitude surface energy balance and can be thought of as a difference in planetary albedo between the Northern and Southern Hemispheres or as a steady deep-ocean circulation that transports energy from the southern to the northern high latitudes. The relatively large amplitude chosen here is necessary to induce sufficiently large ITCZ shifts in our simulations and is not meant to be a faithful representation of the actual antisymmetric component of the annually averaged surface energy budget on Earth. The tropical ocean energy flux divergence with amplitude $\hat{O}_t$ is used in the tropical warming simulations to change the equatorial energy balance. The standard deviation $\delta\phi_t = 4.9°$ confines this component to the equatorial region.

Moist convection is parameterized by a simplified quasi-equilibrium scheme that relaxes temperatures to a moist adiabat and specific humidity to a profile with a fixed reference relative humidity of 70% (O'Gorman and Schneider 2008; Frierson 2007). Large-scale condensation is parameterized so that relative humidity on the grid scale does not exceed 100%. The excess water is removed as precipitation, without reevaporation of condensate.

The GCM's dynamical core integrates the primitive equations spectrally at a horizontal spectral resolution of T85 with 30 unevenly spaced vertical σ levels. The spinup time for the simulations is 2 yr from an isothermal resting state. Time averages are taken over 4 yr after spinup.

a. Global warming simulations

In the global warming simulations, we vary the longwave optical depth $\tau = \eta\tau_{\mathrm{ref}}(\phi)$ by varying the rescaling factor η between 0.4 and 6.0 (18 simulations), as in O'Gorman and Schneider (2008). This results in climates with global-mean surface temperatures between 275 and 315 K. The amplitudes of the symmetric and tropical ocean energy flux divergences are taken to be zero, $\hat{O}_s = \hat{O}_t = 0$. The simulations overestimate the precipitation and circulation strengths for Earth-like global-mean surface temperatures because the symmetric component of the ocean energy transport is zero (Levine and Schneider 2011). We avoid prescribing a fixed symmetric ocean energy flux, because it leads to spurious double ITCZs in cold climates.

b. Tropical warming simulations

In the tropical warming simulations, the optical depth is fixed at $\eta = 1.0$, resulting in climates with an Earth-like global-mean surface temperature of 288 K. The amplitude of the symmetric ocean energy flux divergence is fixed at $\hat{O}_t = 50\,\mathrm{W\,m^{-2}}$, and the amplitude of the tropical ocean energy flux divergence $\hat{O}_t$ is varied between -110 and 10 W m^{-2} (13 simulations). This results in zonal-mean equatorial surface temperatures between 303 and 308 K.

APPENDIX B

Closure Approximations for Eddy Energy Fluxes

a. Closure 1: Diffusing dry static energy and latent energy separately

At the subtropical latitudes where the vertically, zonally, and temporally averaged moist static energy flux $\langle\overline{v}\overline{h}\rangle$ changes sign, we approximate the eddy flux of dry static energy diffusively as

$$\langle\overline{v's'}\rangle \approx \pm c_d c_p \frac{p_0}{g} v_e \cos(\phi_s)\Delta T. \qquad \text{(B1)}$$

Here, c_d is a constant coefficient; $v_e = \sqrt{\mathrm{EKE}\,g/p_0}$, where EKE is the vertically integrated eddy kinetic energy averaged over the hemisphere; and ϕ_s is the latitude of the eddy kinetic energy maximum (i.e., the storm track location). On the right-hand side, we dropped the overbars of zonal- and time-mean quantities to improve readability.

We made the following assumptions in this closure:

- The vertically averaged eddy flux of dry static energy can be represented by near-surface fluxes, and the potential energy flux component $g\langle\overline{v'z'}\rangle$ can be neglected in the

extratropics (it vanishes for geostrophic advecting velocities if the zonal and temporal mean is taken along isobars).
- The near-surface eddy fluxes can be closed diffusively invoking an average eddy velocity.
- The relevant length scale for the diffusive closure is given by the energy-containing length scale of the turbulent velocity field, and mean temperatures vary over the same length scale, assumed to extend from the subtropics to near the poles. (This justifies the use of pole to subtropics temperature differences provided changes in eddy length scales with climate are ignored.)

For the eddy flux of specific humidity q (or latent energy $L_v q$), we use a scaling in terms of the meridional gradient of specific humidity along (dry) isentropes near the surface $\langle\overline{v'q'}\rangle \propto v_e \partial_y q|_\theta$ (Caballero and Langen 2005; O'Gorman and Schneider 2008; Pierrehumbert 2002; Caballero and Hanley 2012). The meridional gradient of specific humidity $q \approx \mathcal{H} q_s$ along isentropes can be re-expressed in terms of the relative humidity $\mathcal{H}$ and the saturation specific humidity q_s. To calculate derivatives of q_s along isentropes, we use the simplified Clausius–Clapeyron relation also used in the GCM,

$$e_s(T) = e_0 \exp\left[-\frac{L_v}{R_v}\left(\frac{1}{T} - \frac{1}{T_0}\right)\right], \tag{B2}$$

where $e_0 = 610.78\,\mathrm{Pa}$, $R_v = 461.5\,\mathrm{J\,K^{-1}\,kg^{-1}}$ is the gas constant of water vapor, and $T_0 = 273.16\,\mathrm{K}$. The saturation vapor pressure and the specific humidity q_s are approximately related by $q_s \approx \epsilon_r e_s/p$, with $\epsilon_r \approx 0.622$ being the ratio of the gas constants of dry air and water vapor. The derivative of q along isentropes is then given by

$$\left.\frac{\partial q}{\partial y}\right|_\theta = \frac{\mathcal{H} q_s}{p}\left(\frac{\epsilon_r L_v}{c_p T} - 1\right)\left.\frac{\partial p}{\partial y}\right|_\theta + q_s \left.\frac{\partial \mathcal{H}}{\partial y}\right|_\theta. \tag{B3}$$

We neglect gradients of relative humidity along isentropes and rewrite the slope of isentropes in terms of meridional gradients of potential temperature $\partial_y\theta$ and static stability $\partial_p\theta$. Averaging over the extratropics introduces the pole to subtropics temperature difference ΔT and the location of the storm track as in Eq. (B1). Because specific humidity decays rapidly with altitude away from the surface, we obtain a scaling for the eddy moisture fluxes at the edges of the tropics in terms of the subtropical near-surface saturation specific humidity and relative humidity,

$$\langle\overline{v'q'}\rangle \approx \pm c_m \frac{p_0}{g} v_e \cos(\phi_s)\Delta T\left(\frac{\epsilon_r L_v}{c_p T} - 1\right)\mathcal{H}\hat{\Gamma} q_s. \tag{B4}$$

Here, c_m is a constant coefficient, $\hat{\Gamma}^{-1} = -p_0\partial_p\theta$ is a static stability measure averaged over the extratropics, and T is a near-surface temperature. We evaluate the near-surface temperature T, relative humidity $\mathcal{H}$, and saturation specific humidity q_s in the subtropics at $\pm 20°$.

In addition to the assumptions made for the dry fluxes, we made the following assumptions for this closure:

- The near-surface turbulent fluxes can be closed via eddy velocities and gradients along isentropes.
- Gradients of relative humidity along isentropes are unimportant for gradients of specific humidity along isentropes.

Combining the closures for the eddy fluxes of dry static energy and latent energy, we obtain the eddy flux of moist static energy in the subtropics,

$$\langle\overline{v'h'}\rangle = \langle\overline{v's'}\rangle(1 + \beta q_s) \tag{B5a}$$

$$= \pm\alpha v_e \Delta T(1 + \beta q_s), \tag{B5b}$$

$$\alpha = c_d c_p \frac{p_0}{g}\cos(\phi_s), \quad \text{and} \tag{B5c}$$

$$\beta = \frac{c_m}{c_d}\frac{L_v}{c_p}\left(\frac{\epsilon_r L_v}{c_p T} - 1\right)\mathcal{H}\hat{\Gamma}. \tag{B5d}$$

Determining the coefficients c_d and c_m by fitting the flux closures to the simulated fluxes at the reference climate with global-mean surface temperature around 288 K gives $c_d \approx 0.03$ and $c_m \approx 0.01$–0.02. Fitting the coefficients to reanalysis data for Earth's atmosphere gives similar results. The differences in c_d and c_m between the hemispheres are around 12% in the GCM simulations and in reanalysis data and so are negligible for our purposes. This closure is used in section 4.

b. Closure 2: Moist static energy diffusion

The above closure Eq. (B5) for the eddy moist static energy flux differs from a diffusive closure for the vertically averaged eddy moist static energy flux: it assumes that the vertically averaged eddy dry static energy flux can be approximated in terms of the meridional temperature gradient, neglecting any vertical structure in dry static energy transport, whereas it explicitly takes into account the vertical structure of the eddy latent energy transport. This is reasonable because specific humidity generally varies much more strongly with height than temperature or dry static energy. Diffusing moist static energy directly without taking into account the vertical structure of specific humidity leads to the following expression for the turbulent moist static energy flux at the edges of the tropics (in terms of near-surface quantities):

$$\langle \overline{v'h'} \rangle \approx \pm c_h \frac{p_0}{g} v_e \cos(\phi_s) \Delta h \tag{B6a}$$

$$= \pm c_h \frac{p_0}{g} v_e \cos(\phi_s)(c_p \Delta T + L_v \Delta q) \tag{B6b}$$

$$= \pm c_h \frac{p_0}{g} v_e \cos(\phi_s)\left(c_p \Delta T + \frac{L_v^2 \mathcal{H} q_s}{R_v T^2} \Delta T\right) \tag{B6c}$$

$$= \pm c_h c_p \frac{p_0}{g} v_e \cos(\phi_s) \Delta T \left(1 + \frac{L_v^2 \mathcal{H}}{c_p R_v T^2} q_s\right) \tag{B6d}$$

$$= \langle \overline{v's'} \rangle (1 + \beta' q_s), \tag{B6e}$$

$$\alpha' = c_h c_p \frac{p_0}{g} v_e \cos(\phi_s), \quad \text{and} \tag{B6f}$$

$$\beta' = \frac{L_v^2 \mathcal{H}}{c_p R_v T^2}. \tag{B6g}$$

Here, $c_h = c_d$ is a dimensionless coefficient and h, T, $\mathcal{H}$, and q are evaluated near the surface. Comparing β from the closure Eq. (B5) with β' from Eq. (B6) reveals the difference between the two approaches. For Earth's climate, $\beta' q_s \approx 1$. The closure Eq. (B6) overestimates the latent energy transport for Earth-like global-mean surface temperatures ($T \approx 290$ K) by 20%–25% in our simulations, but it has the virtue of only requiring one fitting parameter c_h.

For the inferences in section 4, both closure schemes are equally useful. The choice of closure does not affect our conclusions.

REFERENCES

Adler, R. F., and Coauthors, 2003: The Version-2 Global Precipitation Climatology Project (GPCP) monthly precipitation analysis (1979–present). *J. Hydrometeor.,* **4,** 1147–1167, doi:10.1175/1525-7541(2003)004<1147:TVGPCP>2.0.CO;2.

Arbuszewski, J. A., P. B. deMenocal, C. Cléroux, L. Bradtmiller, and A. Mix, 2013: Meridional shifts of the Atlantic intertropical convergence zone since the Last Glacial Maximum. *Nat. Geosci.,* **6,** 959–962, doi:10.1038/ngeo1961.

Berry, G., and M. J. Reeder, 2014: Objective identification of the intertropical convergence zone: Climatology and trends from the ERA-Interim. *J. Climate,* **27,** 1894–1909, doi:10.1175/JCLI-D-13-00339.1.

Broccoli, A. J., K. A. Dahl, and R. J. Stouffer, 2006: Response of the ITCZ to Northern Hemisphere cooling. *Geophys. Res. Lett.,* **33,** L01702, doi:10.1029/2005GL024546.

Caballero, R., and P. L. Langen, 2005: The dynamic range of poleward energy transport in an atmospheric general circulation model. *Geophys. Res. Lett.,* **32,** L02705, doi:10.1029/2004GL021581.

——, and J. Hanley, 2012: Midlatitude eddies, storm-track diffusivity, and poleward moisture transport in warm climates. *J. Atmos. Sci.,* **69,** 3237–3250, doi:10.1175/JAS-D-12-035.1.

Chiang, J. C. H., and C. M. Bitz, 2005: Influence of high latitude ice cover on the marine intertropical convergence zone. *Climate Dyn.,* **25,** 477–496, doi:10.1007/s00382-005-0040-5.

——, and A. R. Friedman, 2012: Extratropical cooling, interhemispheric thermal gradients, and tropical climate change. *Annu. Rev. Earth Planet. Sci.,* **40,** 383–412, doi:10.1146/annurev-earth-042711-105545.

——, M. Biasutti, and D. S. Battisti, 2003: Sensitivity of the Atlantic intertropical convergence zone to Last Glacial Maximum boundary conditions. *Paleoceanography,* **18,** 1094, doi:10.1029/2003PA000916.

Cvijanovic, I., and J. C. H. Chiang, 2013: Global energy budget changes to high latitude North Atlantic cooling and the tropical ITCZ response. *Climate Dyn.,* **40,** 1435–1452, doi:10.1007/s00382-012-1482-1.

Dai, A., and T. M. L. Wigley, 2000: Global patterns of ENSO-induced precipitation. *Geophys. Res. Lett.,* **27,** 1283–1286, doi:10.1029/1999GL011140.

Donohoe, A., J. Marshall, D. Ferreira, and D. McGee, 2013: The relationship between ITCZ location and cross-equatorial atmospheric heat transport: From the seasonal cycle to the Last Glacial Maximum. *J. Climate,* **26,** 3597–3618, doi:10.1175/JCLI-D-12-00467.1.

——, ——, ——, K. Armour, and D. McGee, 2014: The interannual variability of tropical precipitation and interhemispheric energy transport. *J. Climate,* **27,** 3377–3392, doi:10.1175/JCLI-D-13-00499.1.

Fasullo, J. T., and K. E. Trenberth, 2008: The annual cycle of the energy budget. Part II: Meridional structures and poleward transports. *J. Climate,* **21,** 2313–2325, doi:10.1175/2007JCLI1936.1.

Friedman, A. R., Y.-T. Hwang, J. C. H. Chiang, and D. M. W. Frierson, 2013: Interhemispheric temperature asymmetry over the twentieth century and in future projections. *J. Climate,* **26,** 5419–5433, doi:10.1175/JCLI-D-12-00525.1.

Frierson, D. M. W., 2007: The dynamics of idealized convection schemes and their effect on the zonally averaged tropical circulation. *J. Atmos. Sci.,* **64,** 1959–1976, doi:10.1175/JAS3935.1.

——, and Y.-T. Hwang, 2012: Extratropical influence on ITCZ shifts in slab ocean simulations of global warming. *J. Climate,* **25,** 720–733, doi:10.1175/JCLI-D-11-00116.1.

——, I. M. Held, and P. Zurita-Gotor, 2006: A gray-radiation aquaplanet moist GCM. Part I: Static stability and eddy scale. *J. Atmos. Sci.,* **63,** 2548–2566, doi:10.1175/JAS3753.1.

——, and Coauthors, 2013: Contribution of ocean overturning circulation to tropical rainfall peak in the Northern Hemisphere. *Nat. Geosci.,* **6,** 940–944, doi:10.1038/ngeo1987.

Fučkar, N. S., S.-P. Xie, R. Farneti, E. A. Maroon, and D. M. W. Frierson, 2013: Influence of the extratropical ocean circulation on the intertropical convergence zone in an idealized coupled general circulation model. *J. Climate,* **26,** 4612–4629, doi:10.1175/JCLI-D-12-00294.1.

Galewsky, J., A. Sobel, and I. M. Held, 2005: Diagnosis of subtropical humidity dynamics using tracers of last saturation. *J. Atmos. Sci.,* **62,** 3353–3367, doi:10.1175/JAS3533.1.

Ganachaud, A., and C. Wunsch, 2000: Improved estimates of global ocean circulation, heat transport and mixing from hydrographic data. *Nature,* **408,** 453–457, doi:10.1038/35044048.

Haug, G. H., K. A. Hughen, D. M. Sigman, L. C. Peterson, and U. Röhl, 2001: Southward migration of the intertropical convergence zone through the Holocene. *Science,* **293,** 1304–1308, doi:10.1126/science.1059725.

Held, I. M., 2001: The partitioning of the poleward energy transport between the tropical ocean and atmosphere. *J. Atmos. Sci.,* **58,** 943–948, doi:10.1175/1520-0469(2001)058<0943:TPOTPE>2.0.CO;2.

——, and B. J. Soden, 2006: Robust responses of the hydrological cycle to global warming. *J. Climate,* **19,** 5686–5699, doi:10.1175/JCLI3990.1.

Hwang, Y.-T., and D. M. W. Frierson, 2010: Increasing atmospheric poleward energy transport with global warming. *Geophys. Res. Lett.,* **37,** L24807, doi:10.1029/2010GL045440.

——, ——, and S. M. Kang, 2013: Anthropogenic sulfate aerosol and the southward shift of tropical precipitation in the late 20th century. *Geophys. Res. Lett.,* **40,** 2845–2850, doi:10.1002/grl.50502.

Kang, S. M., I. M. Held, D. M. W. Frierson, and M. Zhao, 2008: The response of the ITCZ to extratropical thermal forcing: Idealized slab-ocean experiments with a GCM. *J. Climate,* **21,** 3521–3532, doi:10.1175/2007JCLI2146.1.

——, D. M. W. Frierson, and I. M. Held, 2009: The tropical response to extratropical thermal forcing in an idealized GCM: The importance of radiative feedbacks and convective parameterization. *J. Atmos. Sci.,* **66,** 2812–2827, doi:10.1175/2009JAS2924.1.

Klinger, B. A., and J. Marotzke, 2000: Meridional heat transport by the subtropical cell. *J. Phys. Oceanogr.,* **30,** 696–705, doi:10.1175/1520-0485(2000)030<0696:MHTBTS>2.0.CO;2.

Koutavas, A., and J. Lynch-Stieglitz, 2004: Variability of the marine ITCZ over the eastern Pacific during the past 30,000 years: Regional perspective and global context. *The Hadley Circulation: Present, Past, and Future,* H. F. Diaz and R. S. Bradley, Eds., Springer, 347–369.

Levine, X. J., and T. Schneider, 2011: Response of the Hadley circulation to climate change in an aquaplanet GCM coupled to a simple representation of ocean heat transport. *J. Atmos. Sci.,* **68,** 769–783, doi:10.1175/2010JAS3553.1.

Marshall, J., A. Donohoe, D. Ferreira, and D. McGee, 2013: The ocean's role in setting the mean position of the inter-tropical convergence zone. *Climate Dyn.,* **42,** 1967–1979, doi:10.1007/s00382-013-1767-z.

Mayer, M., and L. Haimberger, 2012: Poleward atmospheric energy transports and their variability as evaluated from ECMWF reanalysis data. *J. Climate,* **25,** 734–752, doi:10.1175/JCLI-D-11-00202.1.

Neelin, J. D., and I. M. Held, 1987: Modeling tropical convergence based on the moist static energy budget. *Mon. Wea. Rev.,* **115,** 3–12, doi:10.1175/1520-0493(1987)115<0003:MTCBOT>2.0.CO;2.

O'Gorman, P. A., and T. Schneider, 2006: Stochastic models for the kinematics of moisture transport and condensation in homogeneous turbulent flows. *J. Atmos. Sci.,* **63,** 2992–3005, doi:10.1175/JAS3794.1.

——, and ——, 2008: The hydrological cycle over a wide range of climates simulated with an idealized GCM. *J. Climate,* **21,** 3815–3832, doi:10.1175/2007JCLI2065.1.

——, N. Lamquin, T. Schneider, and M. S. Singh, 2011: The relative humidity in an isentropic advection–condensation model: Limited poleward influence and properties of subtropical minima. *J. Atmos. Sci.,* **68,** 3079–3093, doi:10.1175/JAS-D-11-067.1.

Pierrehumbert, R. T., 2002: The hydrologic cycle in deep-time climate problems. *Nature,* **419,** 191–198, doi:10.1038/nature01088.

——, H. Brogniez, and R. Roca, 2007: On the relative humidity of the atmosphere. *The Global Circulation of the Atmosphere,* T. Schneider and A. H. Sobel, Eds., Princeton University Press, 143–185.

Rotstayn, L. D., and U. Lohmann, 2002: Tropical rainfall trends and the indirect aerosol effect. *J. Climate,* **15,** 2103–2116, doi:10.1175/1520-0442(2002)015<2103:TRTATI>2.0.CO;2.

Sachs, J. P., D. Sachse, R. H. Smittenberg, Z. Zhang, D. S. Battisti, and S. Golubic, 2009: Southward movement of the Pacific intertropical convergence zone AD 1400–1850. *Nat. Geosci.,* **2,** 519–525, doi:10.1038/ngeo554.

Schneider, T., 2006: The general circulation of the atmosphere. *Annu. Rev. Earth Planet. Sci.,* **34,** 655–688, doi:10.1146/annurev.earth.34.031405.125144.

——, P. A. O'Gorman, and X. J. Levine, 2010: Water vapor and the dynamics of climate changes. *Rev. Geophys.,* **48,** RG3001, doi:10.1029/2009RG000302.

Seager, R., N. Harnik, Y. Kushnir, W. Robinson, and J. Miller, 2003: Mechanisms of hemispherically symmetric climate variability. *J. Climate,* **16,** 2960–2978, doi:10.1175/1520-0442(2003)016<2960:MOHSCV>2.0.CO;2.

Uppala, S. M., and Coauthors, 2005: The ERA-40 Re-Analysis. *Quart. J. Roy. Meteor. Soc.,* **131,** 2961–3012, doi:10.1256/qj.04.176.

Vellinga, M., and R. A. Wood, 2002: Global climatic impacts of a collapse of the Atlantic thermohaline circulation. *Climatic Change,* **54,** 251–267, doi:10.1023/A:1016168827653.

Voigt, A., B. Stevens, J. Bader, and T. Mauritsen, 2013: The observed hemispheric symmetry in reflected shortwave irradiance. *J. Climate,* **26,** 468–477, doi:10.1175/JCLI-D-12-00132.1.

Waliser, D. E., and C. Gautier, 1993: A satellite-derived climatology of the ITCZ. *J. Climate,* **6,** 2162–2174, doi:10.1175/1520-0442(1993)006<2162:ASDCOT>2.0.CO;2.

Walker, C. C., and T. Schneider, 2006: Eddy influences on Hadley circulations: Simulations with an idealized GCM. *J. Atmos. Sci.,* **63,** 3333–3350, doi:10.1175/JAS3821.1.

Yoshimori, M., and A. J. Broccoli, 2008: Equilibrium response of an atmosphere–mixed layer ocean model to different radiative forcing agents: Global and zonal mean response. *J. Climate,* **21,** 4399–4423, doi:10.1175/2008JCLI2172.1.